



OPEN

## Robust sliding-Backstepping mode control of a wind system based on the DFIG generator

Farah Echiheb<sup>1</sup>, Yasmine Ihedrane<sup>1</sup>, Badre Bossoufi<sup>1✉</sup>, Manale Bouderbala<sup>1</sup>, Saad Motahhir<sup>2</sup>, Mehedi Masud<sup>3</sup>, Sultan Aljahdali<sup>3</sup> & Madiha ElGhamrasni<sup>1</sup>

This paper presents a new contribution in the field of the optimization of the techniques of control of the wind systems and the improvement of the quality of energy produced in the grid. The Sliding Mode control technique gives quite interesting results, but its major drawback lies in the phenomenon of chattering (oscillations), which reduces the system's precision. We propose in this work a solution to cancel this chattering phenomenon by the implication of the adaptive Backstepping technique to control the powers of the double-fed asynchronous generator (DFIG) connected to the electrical network by two converters (network side and side machine) in the nominal part of the sliding mode model. This hybrid technique will correct errors of precision and stability and the performance of the wind system obtained in terms of efficiency, active and reactive power is significant. First, a review of the wind system was presented. Then, an exhaustive explanation of the Backstepping technique based on the Lyapunov stability and optimization method has been reported. Subsequently, a validation on the Matlab & Simulink environment was carried out to test the performance and robustness of the proposed model. The results obtained from this work, either by follow-up or robustness tests, show a significant performance improvement compared to other control techniques.

### List of symbols

|                                      |                                          |
|--------------------------------------|------------------------------------------|
| $\Omega_t$                           | Turbine speed                            |
| $R_s, R_r$                           | Stator and rotor resistance              |
| $R_f, L_f$                           | Filter resistance and inductance         |
| $L_r, L_s$                           | Stator and rotor inductance              |
| $P_s, P_r, P_g$                      | Stator and rotor and grid active power   |
| $Q_s, Q_r, Q_g$                      | Stator and rotor and grid reactive power |
| $T_{em}, C_{em}$                     | Electromagnetic torque                   |
| $V_{r(a,b,c)}, V_{s(A,B,C)}$         | Rotor and stator voltages                |
| $i_{r(a,b,c)}, i_{s(A,B,C)}$         | currents of stator and rotor             |
| $(v_{sd}, v_{sq}), (i_{sd}, i_{sq})$ | d/q stator voltages and currents         |
| $(v_{td}, v_{tq}), (i_{td}, i_{tq})$ | Voltages and currents at the RL filter   |

Faced with a growing demand for energy caused by overpopulation throughout the globe and the Monopoly of countries in the industrial field, and the more or less long-term depletion of fossil fuels, traditional energy sources are less and less abundant, and different alternatives have been considered. For example, following the oil crises, some countries have pursued a nuclear-oriented policy while others have massively used renewable energies with the adoption of wind power<sup>1</sup>.

Three significant families are emerging in the field of renewable energies: energies of mechanical origin (wind), energies of electrical origin (photovoltaic panels) or energy in the form of heat (geothermal, solar thermal, etc.). For centuries, wind energy has been used to provide mechanical work. The best-known example is the windmill. In 1888, Charles F. Brush built a small wind turbine to supply his house with electricity, with battery storage<sup>2</sup>.

<sup>1</sup>LIMAS Laboratory, Faculty of Sciences Dhar El Mahraz, Sidi Mohammed Ben Abdellah University, Fez, Morocco. <sup>2</sup>Engineering, Systems, and Applications Laboratory, ENSA, SMBA University, Fez, Morocco. <sup>3</sup>Department of Computer Science, College of Computers and Information Technology, Taif University, P. O. Box 11099, Taif 21944, Saudi Arabia. ✉email: badre.bossoufi@usmba.ac.ma

The displacement of air masses, which is indirectly due to the Earth's sun, generates wind energy. The warming of some areas of the planet and the cooling of others leads to creating a pressure difference and the movement of air masses in a constant way. The energy recovered depends on the wind speed and the surface facing the wind. This energy is used either directly (milling, pumping) or indirectly (electricity production via a generator).

To start a wind turbine, you need a speed of about 15 km/h<sup>3,4</sup>. And for safety reasons, the wind turbine must stop when the wind exceeds 90 km/h. In the nacelle, there is an axis called a shaft driven by the rotor of the alternator. The rotation of the shaft provides energy that allows the alternator to produce an alternating electric current. Depending on the strength of the wind, wind turbines rotate more than 80% of the time at varying speeds. In addition, a wind farm with 4 to 6 wind turbines covers the electricity needs of nearly 12,000 people.

Most wind turbines installed in the past were fixed speed<sup>5,6</sup>. However, these wind turbines have several disadvantages: low energy efficiency and a short lifespan. In addition, this wind turbine technology generates considerable fluctuations in the voltage and power of the network during significant variations in wind speed. Variable-speed wind turbines were then introduced to solve these problems<sup>7,8</sup>.

The most used wind systems in the industry are based on the DFIG double-fed asynchronous generator, given its advantages of size, cost, efficiency, wide operating range (hyper and hypo synchronous), and its acoustic noise in its four-quadrant operation. As a result, they produce high-quality electrical power compared to fixed-speed wind turbines<sup>9</sup>.

Several research works on the control and control of wind turbines have been carried out<sup>10-13</sup>. Nevertheless, the synthesis of these controls from the linear model of the wind turbine degrades performance, especially when faced with a real wind profile<sup>14-16</sup>. This is due to the strongly non-linear aspect of the wind system. Thus, the impact of disturbances on the system is generally not considered with sufficient precision. Consequently, this type of control does not make it possible to maintain good tracking performance in the presence of external disturbances.

This article deals with the modelling, control and simulation of a wind energy conversion system based on a double-fed asynchronous generator (DFIG); this later is connected directly to the grid by its stator and driven by its rotor by two static converters. The idea is to implement a control system decoupled from DFIG to ensure better power quality and make the system insensitive to disturbances.

Our objective in this work is to:

- Develop non-linear modelling of the wind system based on the DFIG
- Apply the classic model of the sliding mode control technique, and highlight its drawback, which is the phenomenon of chattering (oscillations)
- Develop a very robust hybrid control technique with estimators, which is based on a mixture of the Sliding-Backstepping Mode technique, which significantly improves the performance of the wind system in view of the variation of the wind and also the parameter variation of the machine

This paper is organized as follows: after the introduction, a literature review highlights the problem and then the wind system's dynamic modelling (WECS). Next, the design of the hybrid control in sliding-Backstepping mode is proposed. Finally, the simulation results of the proposed control are presented, analyzed, and then compared to the results of other controls.

## Literature review

This section presents some works in the field of control of wind systems, such as classical sliding mode control, direct torque control, and vector control.

Bossoufi et al.<sup>1</sup> This paper discussed a non-linear control applied to a WECS-DFIG and developed the Adaptive Backstepping control based on the Lyapunov stability technique to make WECS works in better conditions.

Yang et al.<sup>2</sup> implemented SMC on DFIG. Unfortunately, the obtained results were inefficient in terms of robustness and set-point follow-up (chattering phenomenon).

Benbouzid et al.<sup>3</sup> presented a high-order sliding mode control technique to a DFIG-based wind system. The high order has improved the performance of the wind system compared to the classical sliding mode control technique, but the results still show oscillations, and the THD remains high.

Djeriri et al.<sup>4</sup> presents a work based on artificial intelligence techniques based on neural networks (DTC-RNA). For a DFIG-based wind system, they combined artificial neural networks with DTC of which hysteresis correctors pose the problem of fluctuations on the different output quantities of the DFIG.

In addition to the previously mentioned non-linear control systems, sliding mode control (SMC) has attracted substantial interest because of its organizational efficiency, fast reaction, ease of implementation, and low sensitivity to parameter changes<sup>14,17</sup>. SMC is a sort of non-linear control that is insensitive to parameter changes. Due to its ease of implementation, order reduction, and tolerance for external disturbances and parametric perturbations, including suitable wind energy extraction, DC link wattage maintenance, and direct wind energy power management, it has attracted considerable interest for WECS control in recent years.

In<sup>18,19</sup>, sliding mode control (SMC) of the first order is utilized to regulate both the speed and power of the PMSG-based WECS. Typically, the current control creates a real-time voltage reference using pulse-width modulation (PWM). The voltage reference cannot be adequately tracked when the sign function is utilized due to the chattering problem. Using continuous approximation and a saturation function for PMSG-based WECS,<sup>18</sup> built an SMC with decreased chattering. Unfortunately, applying a saturation function leads to a finite steady-state error. The authors of<sup>11</sup> provide a way for improving the output power quality using fractional-order sliding mode control (FOSMC); nevertheless, this method requires accurate fractional operator adjustment. The authors of<sup>20</sup> studied a second-order adaptive SMC approach (SOSMC). This method can successfully account for model

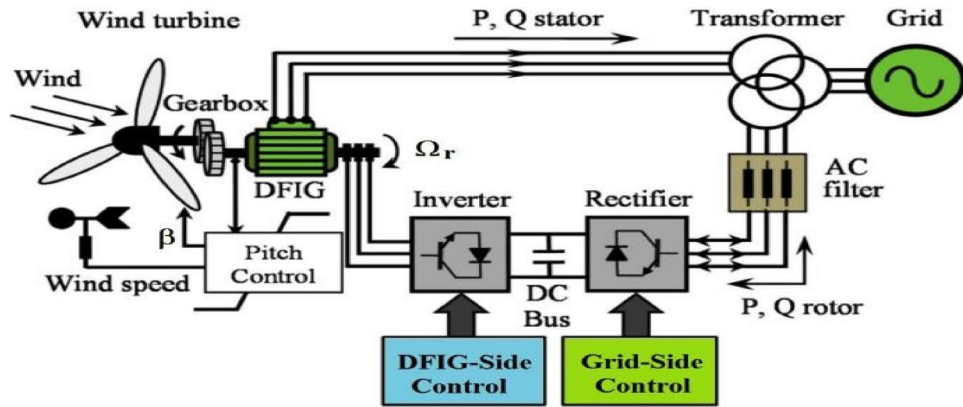


**Figure 1.** WECS based on the DFIG.

error, the inherent nonlinearity of WECS, and random wind. However, due to measurement noise, the use of differentiators demands additional caution.

Meanwhile,<sup>21</sup> described the I-SMC (integral sliding-model control) approach for achieving high-precision steady-state control. However, the controller’s gain must be carefully adjusted to balance volume and noise. In<sup>22</sup>, SOSMC and the Super Twisting (ST) algorithm are merged. Despite the fact that ST can create a quick transient response with low steady-state error, it typically results in high controller gains, which can cause chattering.

Advanced SMC techniques with finite-time convergence have been presented to successfully decrease chattering problems, such as traditional terminal sliding mode control (TSMC) and fast terminal sliding mode control (FTSMC). Both of these solutions rely on non-linear sliding surfaces that incorporate fractional power to enable quick, finite-time convergence during the sliding phase. However, the chattering phenomenon in TSMC and FTSMC is not totally removed, as it is in traditional SMC.

According to these studies, the major problem encountered in most control algorithms was in terms of robustness. Our contribution in this work is to confirm the tracking and regulation performance and then make the wind system insensitive to parametric variations. For that purpose, this study aims to Develop a robust hybrid control technique with estimators, which is based on a mixture of the Sliding-Backstepping Mode technique, which greatly improves the performance of the wind system in view of the variation of the wind and also the parameter variation of the machine.

### Modeling of a wind system based on the DFIG

The turbine transforms the kinetic energy of the wind into mechanical energy. It comprises three identical blades fixed to a drive shaft connected to a speed multiplier having a transformation ratio  $G$ . This multiplier drives the shaft of the electric generator (Fig. 1)<sup>17</sup>.

The generator then provides electrical energy at a variable frequency, and it is necessary to add a power electronics interface between it and the network. This interface is conventionally made up of two converters (a rectifier and an inverter) connected via a DC voltage stage. The grid-side inverter is then decoupled from the machine via the DC bus and there is no direct link between the grid frequency and that delivered by the machine. Such a device must however be designed and controlled in such a way as to limit the disturbances that it is liable to generate on the network. Indeed, the voltage delivered is not sinusoidal and may contain undesirable harmonics. In addition, the converters are sized to transmit all the power exchanged between the generator and the grid; they therefore, represent a financial investment and lead to significant losses<sup>18,19</sup>.

**WECS model.** The turbine is modeled by the following system of equations<sup>17,23</sup>:

$$\begin{cases} P_{aero} = \frac{1}{2} \cdot C_{p-max}(\lambda, \beta) \cdot \rho \cdot \pi \cdot R^2 \cdot v^3 \\ \lambda = \frac{R \cdot \Omega_t}{v} \\ C_{p-Max} = \frac{16}{27} = 0.5925 \\ \frac{1}{\lambda} = \frac{1}{\lambda + 0.008\beta} - \frac{0.035}{\beta^3 + 1} \\ C_p(\lambda, \beta) = C_1 \left( \frac{C_2}{\lambda} - C_3 \cdot \beta - C_4 \right) e^{-\frac{C_5}{\lambda}} + C_6 \end{cases} \quad (1)$$

where  $C_p$ : Power coefficient,  $\lambda$ : Relative speed,  $\beta$ : Pitch angle (deg),  $R$ : Radius of the turbine,  $v$ : Wind speed (m/s),  $\rho$ : Air density ( $1.225 \text{ kg/m}^3$ ).

The turbine is connected to the generator shaft through a gearbox whose model is as follows:

$$\begin{cases} \Omega_t = \frac{\Omega_{mec}}{G} \\ C_g = \frac{C_{aero}}{G} \end{cases} \quad (2)$$

The following mechanical equations model the generator shaft:

$$\begin{cases} J_{\text{tot}} = \frac{J_r}{G^2} + J_g \\ C_{\text{mec}} = J_{\text{tot}} \cdot \frac{d\Omega_{\text{mec}}}{dt} = C_g - C_{\text{em}} - C_f \end{cases} \quad (3)$$

with:  $C_f = f \cdot \Omega_{\text{mec}}$

**DFIG model.** According to the rotating field reference frame of Park, the model of the DFIG is given by the following set of equations<sup>24,20-22,25,26</sup>:

$$\begin{cases} V_{sd} = R_s \cdot I_{sd} + \frac{d\phi_{sd}}{dt} - \omega_s \cdot \phi_{sq} \\ V_{sq} = R_s \cdot I_{sq} + \frac{d\phi_{sq}}{dt} + \omega_s \cdot \phi_{sd} \\ V_{rd} = R_r \cdot I_{rd} + \frac{d\phi_{rd}}{dt} - \omega_r \cdot \phi_{rq} \\ V_{rq} = R_r \cdot I_{rq} + \frac{d\phi_{rq}}{dt} + \omega_r \cdot \phi_{rd} \end{cases} \quad (4)$$

$$\begin{cases} \omega_r = \omega_s - p \cdot \Omega \\ \varphi_{ds} = L_s \cdot i_{ds} + M \cdot i_{dr} \\ \varphi_{qs} = L_s \cdot i_{qs} + M \cdot i_{qr} \\ \varphi_{dr} = L_r \cdot i_{dr} + M \cdot i_{ds} \\ \varphi_{qr} = L_r \cdot i_{qr} + M \cdot i_{qs} \end{cases} \quad (5)$$

$$L_s = l_s - M_s, \quad L_r = l_r - M_r$$

$$C_{\text{em}} = p(\phi_{ds} i_{qs} - \phi_{qs} i_{ds}) \quad (6)$$

$$\begin{cases} P_s = v_{ds} \cdot i_{ds} + v_{qs} \cdot i_{qs} \\ Q_s = v_{qs} \cdot i_{ds} - v_{ds} \cdot i_{qs} \\ P_r = v_{dr} \cdot i_{dr} + v_{qr} \cdot i_{qr} \\ Q_r = v_{qr} \cdot i_{dr} - v_{dr} \cdot i_{qr} \end{cases} \quad (7)$$

## Non-linear control of the WECS based on the DFIG

**The principle of SMC.** The sliding mode control consists of two terms<sup>27,28</sup>: a discontinuous control depending on the sign of the sliding surface and an equivalent control characterizing the dynamics of the sliding surface. The system on the sliding surface:

$$u = u_{\text{eq}} + u_n \quad (8)$$

$u_{\text{eq}}$ : The equivalent control vector describes an ideal sliding motion, i.e. without taking into account the uncertainties and disturbances of the system. It is obtained thanks to the following conditions of invariance of the sliding surface:

$$\begin{cases} \dot{S}(x) = 0 \\ S(x) = 0 \end{cases} \quad (9)$$

In the literature, several choices for the discontinuous control  $u_n$  are proposed; the simplest one is given by:

$$u_n = K \cdot \text{sign}(S(x)) \quad (10)$$

With  $K$  is the control gain.

The expression of the sliding surface is described as follows:

$$S(x) = \left( \frac{d}{dt} + \delta \right)^{r-1} * e(x) \quad (11)$$

$\delta$ : Positive gain that interprets the bandwidth of the desired control.

$e(x)$ : the difference on the variable to be regulated  $e(x) = X_{\text{ref}} - X$ .

$r$ : relative degree, the smallest positive integer representing the number of times that must be differentiated to make the control appear.

The convergence condition is defined by the LYAPUNOV function  $V(x)$ , which makes the surface attractive and invariant<sup>29,30</sup>.

$$V(x) = \frac{1}{2} \cdot S(x)^2 \quad (12)$$

This function is obviously positive definite. The necessary and sufficient condition for the slip variable  $S(x, t)$  to tend to zero is that its derivative be negative definite:

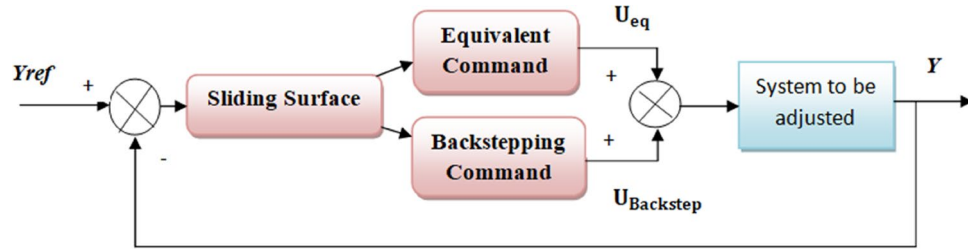


**Figure 2.** Structure of the Sliding-Backstepping Mode Controller.

$$\dot{V}(x) = S(x) * S(x) < 0 \tag{13}$$

The main drawback of this type of control is the phenomenon known as “CHATTERING”<sup>31</sup>. In addition, due to the discontinuous nature of the “SIGN” function, high-frequency oscillations around the equilibrium point appear in a steady-state<sup>32</sup>.

**Hybrid sliding-Backstepping mode control.** To remedy the chattering problem of sliding mode control, we are interested in the new control technique proposed in this article which improves performance and reduces this phenomenon. This technique is called the hybrid Sliding-Backstepping Mode control of DFIG.

The principle of the hybrid control consists in modifying the controller by sliding mode by replacing the stabilizing control  $u_n$  of the sliding mode regulator by the Backstepping controller to solve the CHATTERING problem. The combination of the two parts thus makes it possible to ensure the stability and the robustness of the studied system.

The structure of the Sliding-Backstepping Mode controller is shown in Fig. 2.

This technique is based on decomposing the entire control system, which is usually multivariate and high order into a cascade of first-order control subsystems. Next, a virtual control law is calculated for each subsystem. The latter is considered as a reference for the next subsystem until the control law for the complete system is obtained<sup>33,34</sup>.

*Applying the Backstepping control to the RSC”. Step 1: Calculation of reference rotor currents*

We define the error “ $e_1$ ” and “ $e_2$ ” as follows:

$$\begin{cases} e_1 = P_{sref} - P_s \\ e_2 = Q_{sref} - Q_s \end{cases} \tag{14}$$

$$\begin{cases} \dot{e}_1 = \dot{P}_{sref} - \dot{P}_s \\ \dot{e}_2 = \dot{Q}_{sref} - \dot{Q}_s \end{cases} \tag{15}$$

with:

$$\begin{cases} \dot{P}_s = -\frac{v_s \cdot M}{L_s} \dot{I}_{rq} \\ \dot{Q}_s = \frac{v_s^2}{\omega_s \cdot L_s} - \frac{v_s \cdot M}{L_s} \dot{I}_{rd} \\ \dot{I}_{rd} = \frac{V_{rd}}{L_r \cdot \sigma} - \frac{R_r}{L_r \cdot \sigma} \cdot I_{rd} + \omega_r \cdot I_{rq} \\ \dot{I}_{rq} = \frac{V_{rq}}{L_r \cdot \sigma} - \frac{R_r}{L_r \cdot \sigma} \cdot I_{rq} - \omega_r \cdot I_{rd} - \omega_r \cdot \frac{M \cdot V_s}{L_r \cdot L_s \cdot \sigma \cdot \omega_s} \end{cases} \tag{16}$$

$$\begin{cases} \dot{e}_1 = \dot{P}_{sref} + \frac{V_s \cdot M}{L_s} \left( \frac{V_{rq}}{L_r \cdot \sigma} - \frac{R_r}{L_r \cdot \sigma} \cdot I_{rq} - \omega_r \cdot I_{rd} - \omega_r \cdot \frac{M \cdot V_s}{L_r \cdot L_s \cdot \sigma \cdot \omega_s} \right) \\ \dot{e}_2 = \dot{Q}_{sref} + \frac{V_s \cdot M}{L_s} \left( \frac{V_{rd}}{L_r \cdot \sigma} - \frac{R_r}{L_r \cdot \sigma} \cdot I_{rd} + \omega_r \cdot I_{rq} \right) \end{cases} \tag{17}$$

$$\sigma = 1 - \frac{M^2}{L_s \cdot L_r}$$

The Lyapunov function associated with the errors of the active and reactive power of the stator is given by the following equation:

$$V_1 = \frac{1}{2} e_1^2 + \frac{1}{2} e_2^2 \tag{18}$$

Its derivative is expressed by:

$$\begin{aligned} \dot{V}_1 = e_1 \dot{e}_1 + e_2 \dot{e}_2 = e_1 & \left[ \dot{p}_{sref} + \frac{V_s \cdot M}{L_r \cdot \sigma \cdot L_s} \left( V_{rq} - R_r \cdot I_{rq} - L_r \cdot \sigma \cdot \omega_r \cdot I_{rd} - g \cdot \frac{M \cdot V_s}{L_s} \right) \right] \\ & + e_2 \left[ \dot{q}_{sref} + \frac{V_s \cdot M}{L_r \cdot \sigma \cdot L_s} (V_{rd} - R_r \cdot I_{rd} + L_r \cdot \sigma \cdot \omega_r \cdot I_{rq}) \right] \end{aligned} \quad (19)$$

To ensure the stability of the subsystem, according to Lyapunov  $\dot{V}_1$  must be negative. For this, we choose it in the form<sup>35–37</sup>:

$$\dot{V}_1 = -k_1 e_1^2 - k_2 e_2^2 \leq 0 \quad (20)$$

Performing the equality between Eqs. (19) and (20), we obtain:

$$\begin{aligned} e_1 & \left[ \dot{p}_{sref} + \frac{V_s \cdot M}{L_r \cdot \sigma \cdot L_s} \left( V_{rq} - R_r \cdot I_{rq} - L_r \cdot \sigma \cdot \omega_r \cdot I_{rd} - g \cdot \frac{M \cdot V_s}{L_s} \right) \right] \\ & + e_2 \left[ \dot{q}_{sref} + \frac{V_s \cdot M}{L_r \cdot \sigma \cdot L_s} (V_{rd} - R_r \cdot I_{rd} + L_r \cdot \sigma \cdot \omega_r \cdot I_{rq}) \right] = -k_1 e_1^2 - k_2 e_2^2 \end{aligned} \quad (21)$$

Which give:

$$\begin{aligned} e_1 & \left[ \dot{p}_{sref} + \frac{V_s \cdot M}{L_r \cdot \sigma \cdot L_s} \left( V_{rq} - R_r \cdot I_{rq} - L_r \cdot \sigma \cdot \omega_r \cdot I_{rd} - g \cdot \frac{M \cdot V_s}{L_s} \right) \right] = -k_1 e_1^2 \\ e_2 & \left[ \dot{q}_{sref} + \frac{V_s \cdot M}{L_r \cdot \sigma \cdot L_s} (V_{rd} - R_r \cdot I_{rd} + L_r \cdot \sigma \cdot \omega_r \cdot I_{rq}) \right] = -k_2 e_2^2 \end{aligned} \quad (22)$$

The expression of the virtual control  $I_{rq}$   $I_{rd}$  and  $I_{rd}$  is defined by:

$$\begin{aligned} I_{rqref} & = \left[ \frac{L_r \cdot \sigma \cdot L_s}{R_r \cdot V_s \cdot M} \left( \dot{p}_{sref} + k_1 e_1 + \frac{V_s \cdot M}{L_r \cdot \sigma \cdot L_s} \cdot (V_{rq} - L_r \cdot \sigma \cdot \omega_r \cdot I_{rd} - g \cdot \frac{M \cdot V_s}{L_s}) \right) \right] \\ I_{rdref} & = \frac{L_r \cdot \sigma \cdot L_s}{R_r \cdot V_s \cdot M} \left[ \dot{q}_{sref} + k_2 e_2 + \frac{V_s \cdot M}{L_r \cdot \sigma \cdot L_s} (V_{rd} + L_r \cdot \sigma \cdot \omega_r \cdot I_{rq}) \right] \end{aligned} \quad (23)$$

This will be the desired system reference that follows.

#### Step 2: Calculation of rotor voltages

We will deduce the true control law  $V_{rqn}$  and  $V_{rdn}$  which makes it possible to achieve the design objectives for the overall system.

The rotor current errors are defined by<sup>38, 39</sup>:

$$\begin{cases} e_3 = I_{rqref} - I_{rq} \\ e_4 = I_{rdref} - I_{rd} \end{cases} \quad (24)$$

Their derivatives are given by:

$$\begin{cases} \dot{e}_3 = \dot{I}_{rqref} - \dot{I}_{rq} \\ \dot{e}_4 = \dot{I}_{rdref} - \dot{I}_{rd} \end{cases} \quad (25)$$

So:

$$\begin{aligned} \dot{e}_3 & = \dot{I}_{rqref} - \frac{1}{L_r \cdot \sigma} (V_{rqn} - R_r \cdot I_{rq} - L_r \cdot \sigma \cdot \omega_r \cdot I_{rd} - g \cdot \frac{M \cdot V_s}{L_s}) \\ \dot{e}_4 & = \dot{I}_{rdref} - \frac{1}{L_r \cdot \sigma} (V_{rdn} - R_r \cdot I_{rd} + L_r \cdot \sigma \cdot \omega_r \cdot I_{rq}) \end{aligned} \quad (26)$$

The extended Lyapunov function becomes as follows:

$$V_2 = \frac{1}{2} e_1^2 + \frac{1}{2} e_2^2 + \frac{1}{2} e_3^2 + \frac{1}{2} e_4^2 \quad (27)$$

Its derivative is given by:

$$\dot{V}_2 = e_1 \dot{e}_1 + e_2 \dot{e}_2 + e_3 \dot{e}_3 + e_4 \dot{e}_4 \quad (28)$$

Which give:

$$\begin{aligned} \dot{V}_2 = \dot{V}_1 + e_3 \dot{e}_3 + e_4 \dot{e}_4 = \dot{V}_1 + e_3 & \left[ \dot{I}_{rqref} - \frac{1}{L_r \cdot \sigma} \left( V_{rqn} - R_r \cdot I_{rq} - L_r \cdot \sigma \cdot \omega_r \cdot I_{rd} - g \cdot \frac{M \cdot V_s}{L_s} \right) \right] \\ & + e_4 \left[ \dot{I}_{rdref} - \frac{1}{L_r \cdot \sigma} (V_{rdn} - R_r \cdot I_{rd} + L_r \cdot \sigma \cdot \omega_r \cdot I_{rq}) \right] \end{aligned} \quad (29)$$

$\dot{V}_2$  must be negative for the system to be stable. For this, we choose  $\dot{V}_2$  in the form:

$$\dot{V}_2 = -k_1 e_1^2 - k_2 e_2^2 - k_3 e_3^2 - k_4 e_4^2 = \dot{V}_1 - k_3 e_3^2 - k_4 e_4^2 \leq 0 \quad (30)$$

By making the equality between (29) and (30), we obtain:

$$\begin{aligned} \dot{V}_1 - k_3 e_3^2 - k_4 e_4^2 = \dot{V}_1 + e_3 \left[ \dot{I}_{rqref} - \frac{1}{L_r \sigma} (V_{rqn} - R_r I_{rq} - L_r \sigma \omega_r I_{rd} - g \frac{M V_s}{L_s}) \right] \\ + e_4 \left[ \dot{I}_{rdref} - \frac{1}{L_r \sigma} (V_{rdn} - R_r I_{rd} + L_r \sigma \omega_r I_{rq}) \right] \end{aligned} \tag{31}$$

So:

$$\begin{aligned} e_3 \left[ \dot{I}_{rqref} - \frac{1}{L_r \sigma} (V_{rqn} - R_r I_{rq} - L_r \sigma \omega_r I_{rd} - g \frac{M V_s}{L_s}) \right] = -k_3 e_3^2 \\ e_4 \left[ \dot{I}_{rdref} - \frac{1}{L_r \sigma} (V_{rdn} - R_r I_{rd} + L_r \sigma \omega_r I_{rq}) \right] = -k_4 e_4^2 \end{aligned} \tag{32}$$

Which gives the expression of the global real control  $V_{rqn}$  and  $V_{rdn}$  defined by:

$$\begin{cases} V_{rdn} = L_r \sigma \left[ k_4 e_4 + \dot{I}_{rdref} + \frac{1}{L_r \sigma} (R_r I_{rd} - L_r \sigma \omega_r I_{rq}) \right] \\ V_{rqn} = L_r \sigma \left[ k_3 e_3 + \dot{I}_{rqref} + \frac{1}{L_r \sigma} (R_r I_{rq} + L_r \sigma \omega_r I_{rd} + g \frac{M V_s}{L_s}) \right] \end{cases} \tag{33}$$

With:  $k_3, k_4$  are positive constants.

Applying the Backstepping control to the GSC. **Step 1:** Calculation of filter currents  $I_{fd}$  and  $I_{fq}$   
The active and reactive power errors of the filter are given by:

$$\begin{cases} e_5 = P_{fref} - P_f \\ e_6 = Q_{fref} - Q_f \end{cases} \tag{34}$$

The derivatives of the errors are as follows:

$$\begin{cases} \dot{e}_5 = \dot{P}_{fref} - \dot{P}_f \\ \dot{e}_6 = \dot{Q}_{fref} - \dot{Q}_f \end{cases} \tag{35}$$

With :

$$\begin{cases} P_f = v_s I_{qf} \\ Q_f = -v_s I_{df} \\ \dot{I}_{qf} = -\frac{v_{qfn}}{L_f} - \frac{R_f}{L_f} I_{qf} - \omega_s I_{df} + \frac{v_s}{L_f} \\ \dot{I}_{df} = -\frac{v_{dfn}}{L_f} - \frac{R_f}{L_f} I_{df} + \omega_s I_{qf} \end{cases} \tag{36}$$

Substituting (36) into (35), we get the following equation:

$$\begin{cases} \dot{e}_5 = \dot{P}_{fref} - v_s \left( -\frac{v_{qfn}}{L_f} - \frac{R_f}{L_f} I_{qf} - \omega_s I_{df} + \frac{v_s}{L_f} \right) \\ \dot{e}_6 = \dot{Q}_{fref} + v_s \left( -\frac{v_{dfn}}{L_f} - \frac{R_f}{L_f} I_{df} + \omega_s I_{qf} \right) \end{cases} \tag{37}$$

The Lyapunov function associated with the errors of the active and reactive power of the filter is given by the following equation<sup>40</sup>:

$$V_3 = \frac{1}{2} e_5^2 + \frac{1}{2} e_6^2 \tag{38}$$

Its derivative is given by:

$$\dot{V}_3 = e_5 \dot{e}_5 + e_6 \dot{e}_6 = e_5 \left( \dot{P}_{fref} - v_s \left( -\frac{v_{qfn}}{L_f} - \frac{R_f}{L_f} I_{qf} - \omega_s I_{df} + \frac{v_s}{L_f} \right) \right) + e_6 \left( \dot{Q}_{fref} + v_s \left( -\frac{v_{dfn}}{L_f} - \frac{R_f}{L_f} I_{df} + \omega_s I_{qf} \right) \right) \tag{39}$$

$\dot{V}_3$  must be negative for the system to be stable. For this, we choose  $\dot{V}_3$  in the form:

$$\dot{V}_3 = -k_5 e_5^2 - k_6 e_6^2 \leq 0 \tag{40}$$

With:  $k_5, k_6$  are positive constants.

By making the equality between (39) and (40), we obtain:

$$e_5 \left( \dot{P}_{fref} - v_s \left( -\frac{v_{qfn}}{L_f} - \frac{R_f}{L_f} I_{qf} - \omega_s I_{df} + \frac{v_s}{L_f} \right) \right) + e_6 \left( \dot{Q}_{fref} + v_s \left( -\frac{v_{dfn}}{L_f} - \frac{R_f}{L_f} I_{df} + \omega_s I_{qf} \right) \right) = -k_5 e_5^2 - k_6 e_6^2 \tag{41}$$

Which give:

$$\begin{cases} e_5 \left( \dot{P}_{fref} - v_s \left( -\frac{v_{qfn}}{L_f} - \frac{R_f}{L_f} I_{qf} - \omega_s I_{df} + \frac{v_s}{L_f} \right) \right) = -k_5 e_5^2 \\ e_6 \left( \dot{Q}_{fref} + v_s \left( -\frac{v_{dfn}}{L_f} - \frac{R_f}{L_f} I_{df} + \omega_s I_{qf} \right) \right) = -k_6 e_6^2 \end{cases} \tag{42}$$

The expression of the virtual control  $I_{qf}$  and  $I_{df}$  is defined by:

$$\begin{cases} I_{qfref} = -\frac{L_f}{R_f \cdot v_s} \left( \dot{P}_{fref} + v_s \left( \frac{v_{qfn}}{L_f} + \omega_s I_{df} - \frac{v_s}{L_f} \right) + k_5 e_5 \right) \\ I_{dfref} = \frac{L_f}{R_f \cdot v_s} \left( \dot{Q}_{fref} + v_s \cdot \left( -\frac{v_{dfn}}{L_f} + \omega_s I_{qf} \right) + k_6 e_6 \right) \end{cases} \quad (43)$$

This control will be the desired reference of the following system.

**Step 2:** Calculation of the filter voltages  $V_{fdn}$  and  $V_{fqn}$

In this step, we will deduce the true control law  $V_{fdn}$  and  $V_{fqn}$  to achieve the design objectives for the overall system<sup>41, 42</sup>.

$$\begin{cases} e_7 = I_{dfref} - I_{df} \\ e_8 = I_{qfref} - I_{qf} \end{cases} \quad (44)$$

The derivatives of the errors are given by:

$$\begin{cases} \dot{e}_7 = \dot{I}_{dfref} - \dot{I}_{df} \\ \dot{e}_8 = \dot{I}_{qfref} - \dot{I}_{qf} \end{cases} \quad (45)$$

By replacing (43) in (45), we obtain the following equation:

$$\begin{cases} \dot{e}_7 = \dot{I}_{dfref} + \frac{v_{dfn}}{L_f} + \frac{R_f}{L_f} I_{df} - \omega_s I_{qf} \\ \dot{e}_8 = \dot{I}_{qfref} + \frac{v_{qfn}}{L_f} + \frac{R_f}{L_f} I_{qf} + \omega_s I_{df} - \frac{v_s}{L_f} \end{cases} \quad (46)$$

We first choose the candidate function of “LYAPUNOV” associated with the errors of the filter currents in the following quadratic form:

$$V_4 = \frac{1}{2} e_7^2 + \frac{1}{2} e_8^2 \quad (47)$$

Its derivative is given by:

$$\dot{V}_4 = e_7 \dot{e}_7 + e_8 \dot{e}_8 = e_7 \left( \dot{I}_{dfref} + \frac{v_{dfn}}{L_f} + \frac{R_f}{L_f} I_{df} - \omega_s I_{qf} \right) + e_8 \left( \dot{I}_{qfref} + \frac{v_{qfn}}{L_f} + \frac{R_f}{L_f} I_{qf} + \omega_s I_{df} - \frac{v_s}{L_f} \right) \quad (48)$$

According to LYAPUNOV, it is necessary to choose a negative function  $\dot{V}_4$ , to ensure the stability of the system. For this, we choose  $\dot{V}_4$  in the following form:

$$\dot{V}_4 = -k_7 e_7^2 - k_8 e_8^2 \leq 0 \quad (49)$$

With:  $k_7, k_8$  are positive constants.

Equations (48) and (49), we get:

$$e_7 \left( \dot{I}_{dfref} + \frac{v_{dfn}}{L_f} + \frac{R_f}{L_f} I_{df} - \omega_s I_{qf} \right) + e_8 \left( \dot{I}_{qfref} + \frac{v_{qfn}}{L_f} + \frac{R_f}{L_f} I_{qf} + \omega_s I_{df} - \frac{v_s}{L_f} \right) = -k_7 e_7^2 - k_8 e_8^2 \quad (50)$$

Which give:

$$\begin{cases} e_7 \left( \dot{I}_{dfref} + \frac{v_{dfn}}{L_f} + \frac{R_f}{L_f} I_{df} - \omega_s I_{qf} \right) = -k_7 e_7^2 \\ e_8 \left( \dot{I}_{qfref} + \frac{v_{qfn}}{L_f} + \frac{R_f}{L_f} I_{qf} + \omega_s I_{df} - \frac{v_s}{L_f} \right) = -k_8 e_8^2 \end{cases} \quad (51)$$

The expression of the real global control  $V_{qfn}$  and  $V_{fdn}$  defined by:

$$\begin{cases} v_{dfn} = -L_f (k_7 e_7 + \dot{I}_{dfref} + \frac{R_f}{L_f} I_{df} + \omega_s I_{qf}) \\ v_{qfn} = -L_f (k_8 e_8 + \dot{I}_{qfref} + \frac{R_f}{L_f} I_{qf} + \omega_s I_{df} - \frac{v_s}{L_f}) \end{cases} \quad (52)$$

**Generation of the global control by the sliding-Backstepping mode control.** The Sliding-Backstepping Mode controller is composed of two parts: the first “ $u_{eq}$ ” generated by the sliding mode control and the second “ $u_n$ ” generated by the Backstepping control [43–46].

$$u_{MG-BS} = u_{eq-MG} + u_{n-BS} \quad (53)$$

We will apply the same sliding mode control structure studied in the previous part to generate the equivalent control  $u_{eq-MG}$ , and in the second part  $u_{n-BS}$  we will use the Backstepping control to have the stabilizing control  $U_n$ .

*Application of the hybrid control to the RSC.* By applying the Hybrid Sliding-Backstepping Mode control to the Rotor Side Converter, the global equation of the  $V_{rd}$  and  $V_{rq}$  control takes the following forms<sup>47, 48</sup>:

The voltage  $V_{rd}$  having the equation:



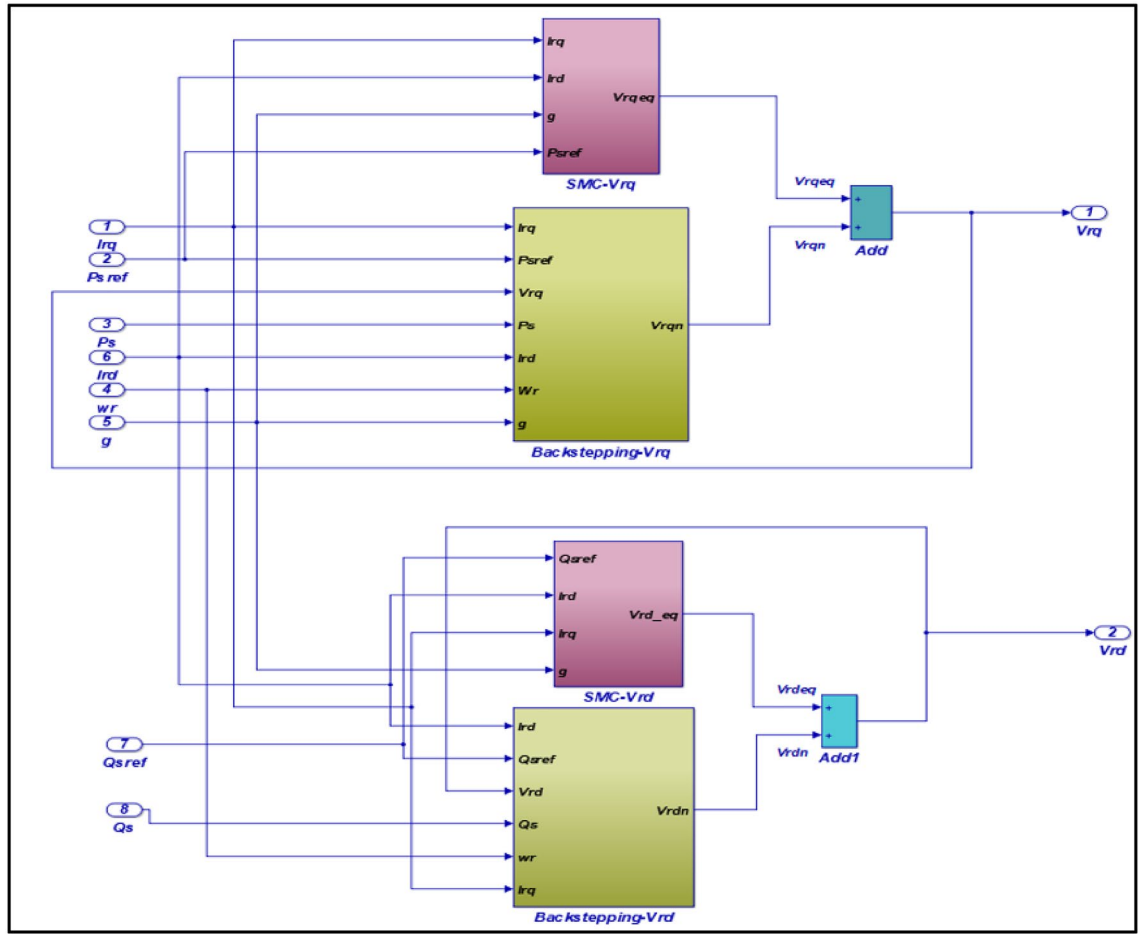


**Figure 3.** Sliding-Backstepping mode control applied to the RSC.

$$V_{rd} = -\frac{L_r \cdot L_s \cdot \sigma}{M \cdot V} \cdot \dot{Q}_{sref} + R_r \cdot I_{rd} - L_r \cdot \sigma \cdot \omega_r \cdot I_{rq} + L_r \cdot \sigma \left[ k_4 e_4 + \dot{I}_{rdref} + \frac{1}{L_r \cdot \sigma} (R_r \cdot I_{rd} - L_r \cdot \sigma \cdot \omega_r \cdot I_{rq}) \right] \quad (54)$$

The given voltage  $V_{rq}$ :

$$V_{rq} = -\frac{L_r \cdot L_s \cdot \sigma}{M \cdot V} \cdot \dot{P}_{sref} + R_r \cdot I_{rq} + L_r \cdot \sigma \cdot \omega_r \cdot I_{rd} + \omega_r \cdot M \cdot \frac{M \cdot V_s}{L_s \cdot \omega_s} + L_r \cdot \sigma \left[ k_3 e_3 + \dot{I}_{rqref} + \frac{1}{L_r \cdot \sigma} (R_r \cdot I_{rq} + L_r \cdot \sigma \cdot \omega_r \cdot I_{rd} + g \cdot \frac{M \cdot V_s}{L_s}) \right] \quad (55)$$

According to the voltage equations, we elaborate the control block by the Sliding-Backstepping Mode applied to the RSC illustrated by the following Fig. 3.

*Application of the hybrid control to the GSC.* By applying the Hybrid Sliding-Backstepping Mode control to the Grid Side Converter, the expression of the Global control  $v_{df}$  and  $v_{qf}$  is given by:

$$\begin{cases} v_{df} = \frac{L_f}{V_s} \dot{Q}_{sref} - R_f I_{df} + L_f I_{qf} \omega_s - L_f (k_5 e_5 + \dot{I}_{dfref} + \frac{R_f}{L_f} I_{df} + \omega_s I_{qf}) \\ v_{qf} = \frac{L_f}{V_s} \dot{P}_{sref} - R_f I_{qf} - L_f I_{df} \omega_s + v_s - L_f (k_6 e_6 + \dot{I}_{qfref} + \frac{R_f}{L_f} I_{qf} + \omega_s I_{df} - \frac{v_s}{L_f}) \end{cases} \quad (56)$$

The control block by the Sliding-Backstepping Mode control applied to the GSC is given by the following Fig. 4.

**Simulation results**

To illustrate the performance of the Sliding-Backstepping Mode control applied to a 10 kW DFIG connected to a 400V / 50Hz Grid dedicated to a wind system, we will apply the same tests carried out previously.

*Pursuit tests.* Step speed response. Variable speed response. From these results (Figs. 5 and 6), we can conclude that the powers generated by the DFIG perfectly follow their references with better decoupling and a low response time lower than that of the PI regulator and the sliding mode regulator.

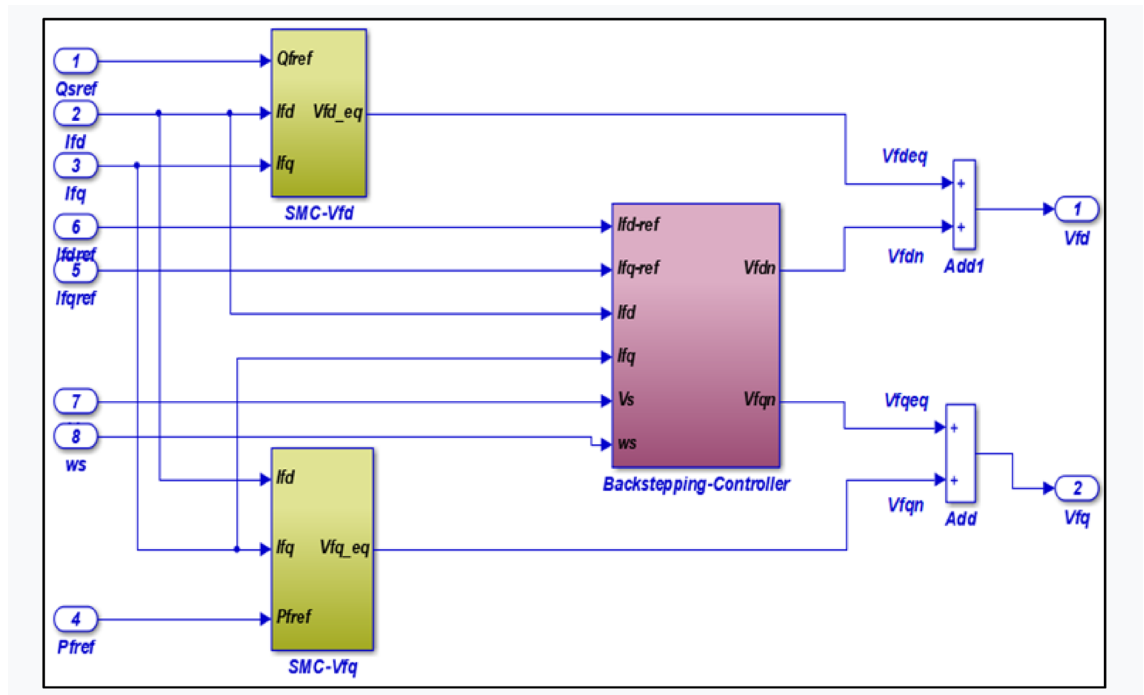


**Figure 4.** Sliding-Backstepping mode control applied to GSC.

We can also notice that the electromagnetic torque depends on the active power, this is translated by its form identical to that of the active power.

The rotor current  $I_{rq}$  depends on the Active power  $P_s$  and the rotor current  $I_{rd}$  depends on the Reactive power  $Q_s$ .

The positive sign of the slip  $g$  then indicates that the machine is operating in hypo-synchronous mode.

The GRID receives good quality energy because, according to the results obtained, the currents of the  $I_{Sabc}$  stator are sinusoidal, of better quality than those obtained by the control of the sliding mode.

Figure 6 shows that the DC bus voltage perfectly follows its reference value of 510 V with almost zero error and a slower response time than the sliding mode control.

Table 1 summarizes the response time of the controller by Sliding-Backstepping Mode for the active and reactive powers as well as the DC-bus voltage.

One can also see that the results obtained from the Sliding-Backstepping Mode control are less wavy than the control results by sliding mode, which implies the robustness of the proposed control.

**Robustness tests.** The same tests were carried out to test the robustness of the DFIG Sliding-Backstepping Mode control:  $R_r$  and  $R_s$  increase by 50% of their nominal values. The results obtained are represented through Figs. 7 and 8:

*Step wind speed response.* Response to variable wind speed. The simulation results (Figs. 7 and 8) show the robustness of the Sliding-Backstepping Mode control compared to the parametric variations of the DFIG. This is justified by the good monitoring of the power set points, with almost the same response time at startup. Furthermore, the active and reactive powers are always kept decoupled.

**Spectral analysis by the Sliding-Backstepping Mode control.** The results of Fig. 9 show the efficiency of the proposed Hybrid control concerning the reduction of the CHATTERING phenomenon, this is justified by the decrease in the rate of harmonic distortion THD which equals 1.19% for the current rotor of one phase and 0.87% for the stator current  $I_{sa}$ .

These results allow us to conclude that the Sliding-Backstepping controller is the most efficient concerning reducing the CHATTERING phenomenon and the most robust concerning the parametric variations of the machine (Table 2).

## Conclusions

Initially, the WECS and the DFIG models were developed, then and given keeping the robustness of the sliding mode control of a wind energy conversion system based on DFIG and eliminating the phenomenon of CHATTERING without degrading the performance of the system, hybridization between the sliding mode control and the Backstepping control was evaluated.

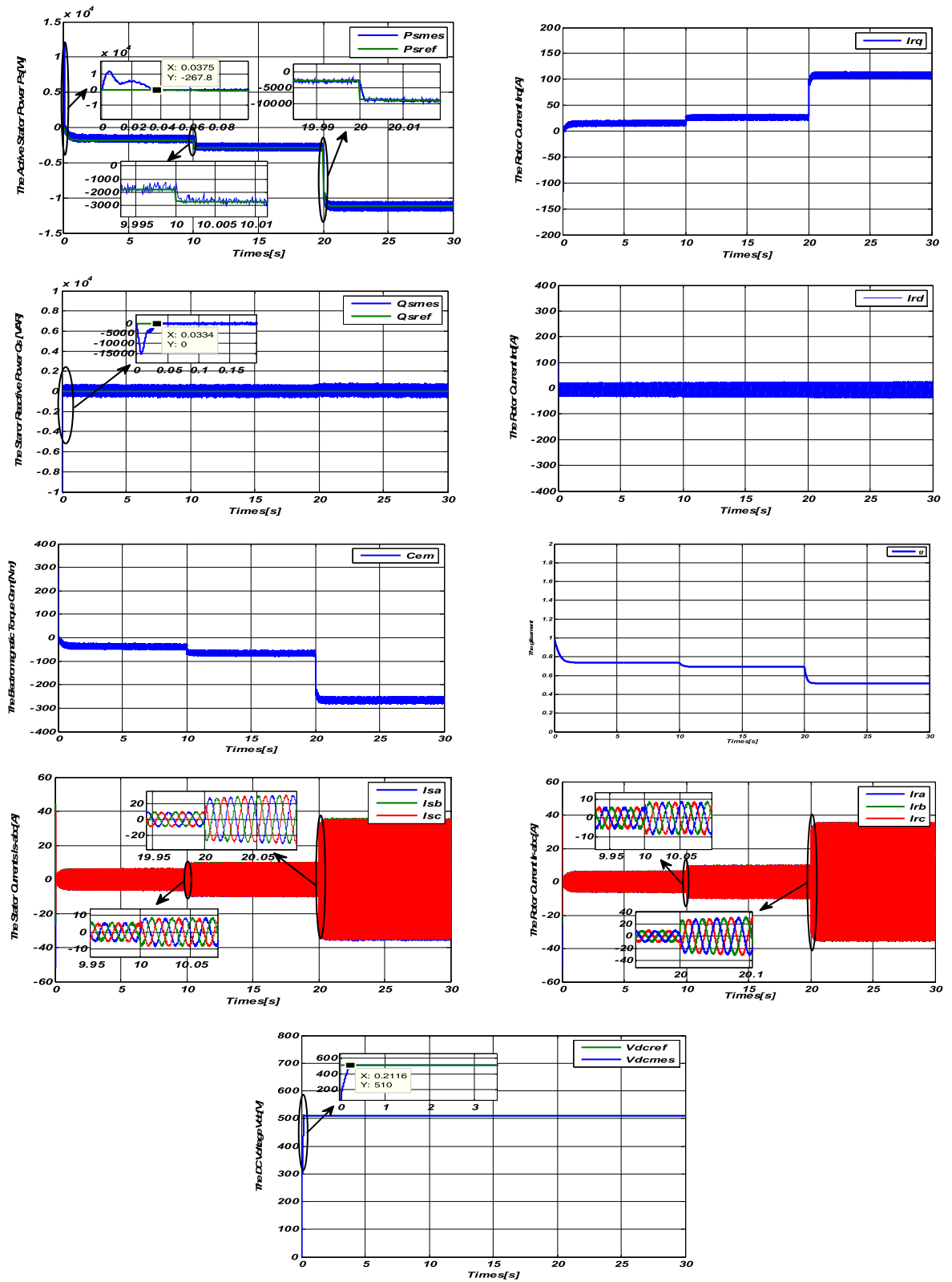
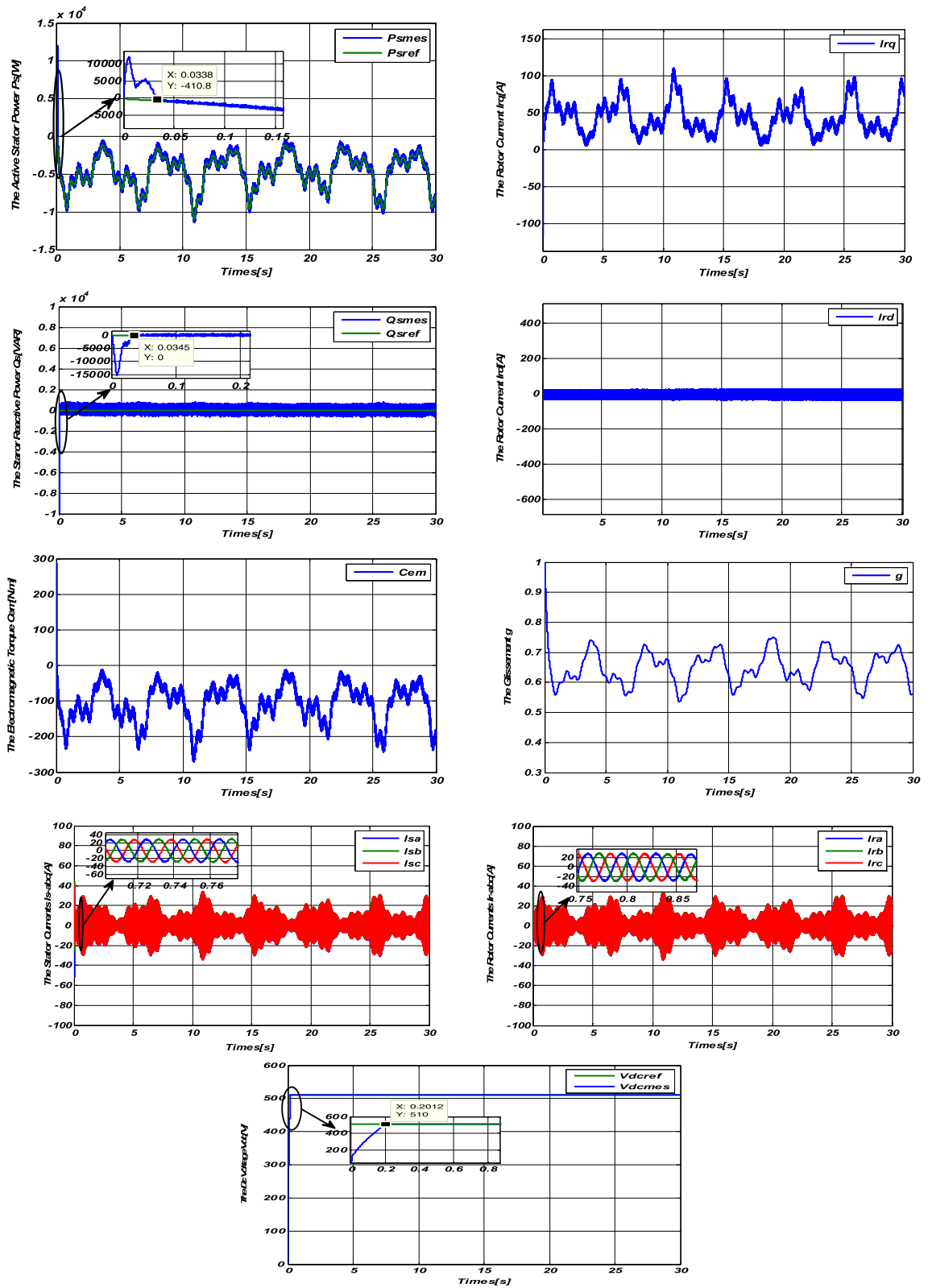


Figure 5. Results of the Sliding-Backstepping Mode control at step wind speed”.

This hybridization technique has given rise to a new robust regulator called drag Backstepping mode. The control is then reviewed to ensure that the WECS extracts the maximum amount of electrical energy towards parametric variations. Next, a simulation was run in Matlab/Simulink environments to determine the performance and durability of the proposed control.



**Figure 6.** Results of the Sliding-Backstepping Mode variable speed control.

The results obtained showed very satisfactory and significant performance of good regulation. In addition, the pursuit, regulation, and robustness behaviours are significantly better than those observed for the other strategies studied.

| MG-BS controller  | tr     |
|-------------------|--------|
| Active Power Ps   | 0.0338 |
| Reactive Power Qs | 0.0345 |
| DC-Bus            | 0.2012 |

**Table 1.** summary of Backstepping controller response time.

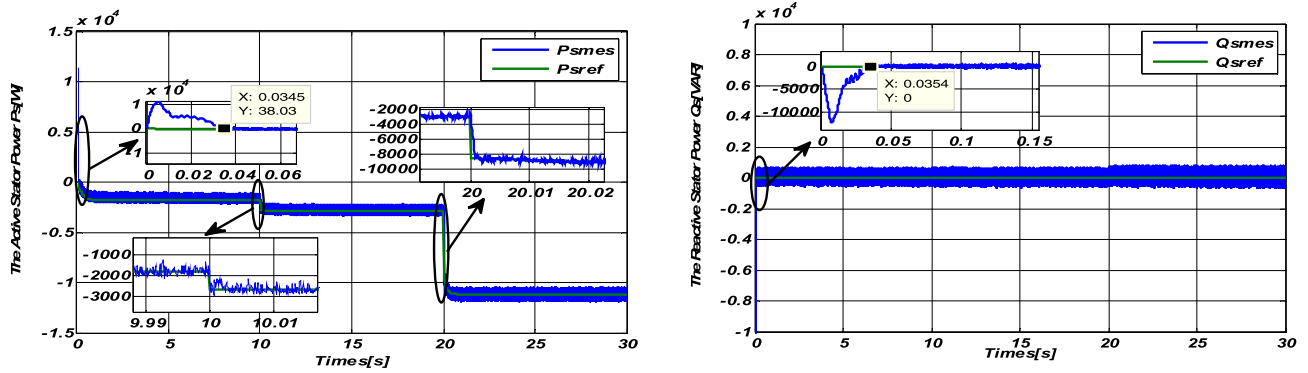


**Figure 7.** Robustness test with variation of resistances  $R_r$  and  $R_s$  for step wind speed.

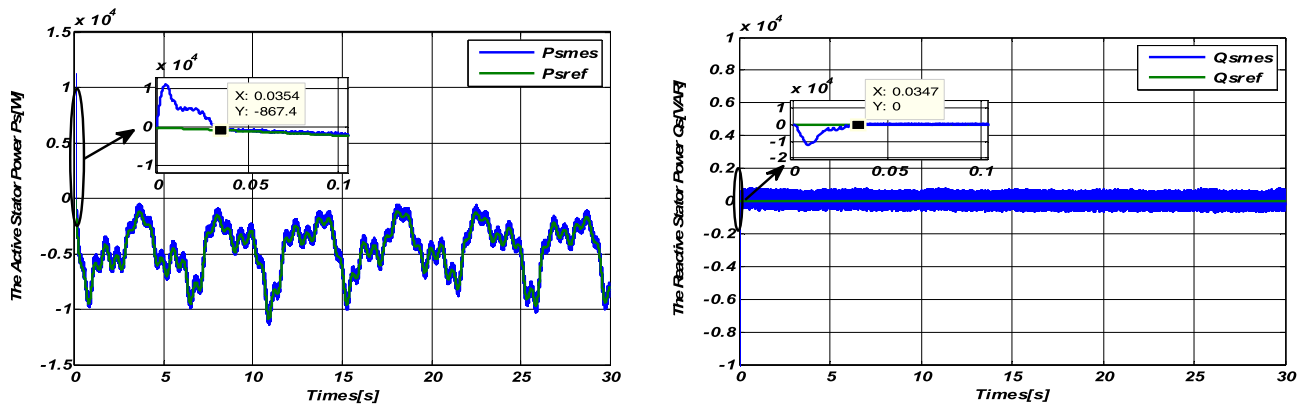


**Figure 8.** Robustness test with the variation of resistances  $R_r$  and  $R_s$  for variable wind speed.

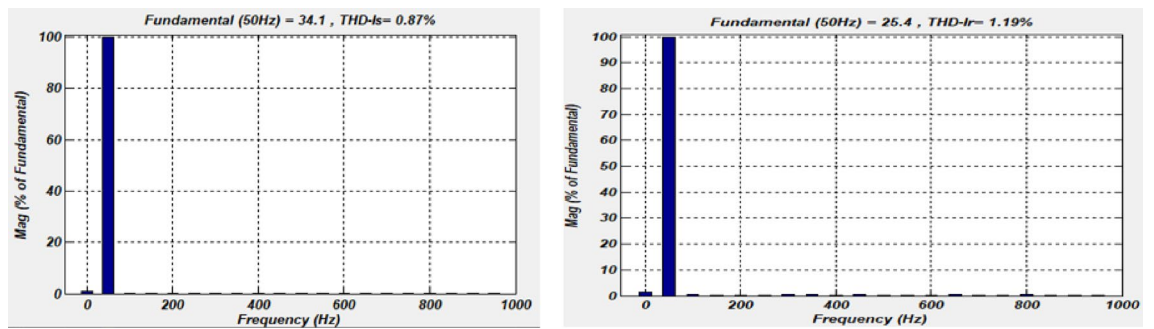


**Figure 9.** Spectral analysis of the phase current  $I_{sa}$  and  $I_{ra}$  using the Sliding-Backstepping Mode control.

As a perspective, the proposed method will be implemented in an embedded board to build a prototype that can be commercialized, and also develop a new control method by applying the proposed method to the finite/ fixed time SMC method.

| Publication paper  | Technical methods                    | Response time(s) | Error (%) | THD (%) |
|--------------------|--------------------------------------|------------------|-----------|---------|
| <sup>5</sup>       | Fuzzy field-oriented control         | 1                | –         | 1.54    |
| <sup>8</sup>       | Direct Control                       | –                | –         | 1.60    |
| <sup>11</sup>      | Model predictive speed control       | 0.0896           | –         | –       |
| <sup>17</sup>      | Double Integral Sliding Mode control | 0.003            | 0.006     | 1.39    |
| <sup>49</sup>      | Proposed Sliding Mode control        | 0.015            | 0.15      | 1.25    |
| Proposed technique | B-SMC                                | 0.03             | 0.09      | 0.87    |

**Table 2.** Control's comparison.

## Data availability

Data available on request from the authors.

Received: 22 March 2022; Accepted: 1 July 2022

Published online: 12 July 2022

## References

- Bossoufi, B. *et al.* DSPACE-based implementation for observer backstepping power control of DFIG wind turbine. *IET Electr. Power Appl.* **14**(12), 2395–2403. <https://doi.org/10.1049/iet-epa.2020.0364> (2020).
- Yang, B., Yu, T., Shu, H., Dong, J. & Jiang, L. Robust sliding-mode control of wind energy conversion systems for optimal power extraction via non-linear perturbation observers. *Appl. Energy* **210**, 711–723 (2018).
- Benamor, A., Benchouia, M. T., Srairi, K. & Benbouzid, M. E. H. A new rooted tree optimization algorithm for indirect power control of wind turbine based on a doubly-fed induction generator. *ISA Trans.* **88**, 296–306 (2019).
- Youness, E. M. *et al.* Implementation and validation of backstepping control for PMSG wind turbine using dSPACE controller board. *Energy Rep.* **5**, 807–821. <https://doi.org/10.1016/j.egy.2019.06.015> (2019).
- Hong, C. M., Chen, C. H. & Tu, C. S. Maximum power point tracking-based control algorithm for PMSG wind generation system without mechanical sensors. *Energy Convers. Manag.* **69**, 58–67. <https://doi.org/10.1016/j.enconman.2012.12.012> (2013).
- Benamor, A., Benchouia, M. T., Srairi, K. & Benbouzid, M. E. H. A novel rooted tree optimization apply in the high order sliding mode control using super-twisting algorithm based on DTC scheme for DFIG. *Int. J. Electr. Power Energy Syst.* **108**(January), 293–302. <https://doi.org/10.1016/j.ijepes.2019.01.009> (2019).
- Pan, L. & Shao, C. Wind energy conversion systems analysis of PMSG on offshore wind turbine using improved SMC and Extended State Observer. *Renew. Energy* **161**, 149–161. <https://doi.org/10.1016/j.renene.2020.06.057> (2020).
- Boumar, N., Labdai, S. & Boulkroune, A. PSO–GSA based fuzzy sliding mode controller for DFIG-based wind turbine. *ISA Trans.* **85**, 177–188. <https://doi.org/10.1016/j.isatra.2018.10.020> (2019).
- Liu, J., Zhou, F., Zhao, C., Wang, Z. & Aguirre-Hernandez, B. A PI-type sliding mode controller design for PMSG-based wind turbine. *Complexity* <https://doi.org/10.1155/2019/2538206> (2019).
- Soliman, M. A., Hasanien, H. M., Azazi, H. Z., El-Kholy, E. E. & Mahmoud, S. A. An adaptive fuzzy logic control strategy for performance enhancement of a grid-connected PMSG-Based wind turbine. *IEEE Trans. Ind. Inform.* **15**(6), 3163–3173. <https://doi.org/10.1109/TII.2018.2875922> (2019).
- Beddar, A., Bouzekri, H., Babes, B. & Afghoul, H. Experimental enhancement of fuzzy fractional order PI+I controller of grid connected variable speed wind energy conversion system. *Energy Convers. Manag.* **123**, 569–580. <https://doi.org/10.1016/j.enconman.2016.06.070> (2016).
- Aounallah, T., Essounbouli, N., Hamzaoui, A. & Bouchafaa, F. Algorithm on fuzzy adaptive backstepping control of fractional order for doubly-fed induction generators. *IET Renew. Power Gener.* **12**(8), 962–967. <https://doi.org/10.1049/iet-rpg.2017.0342> (2018).
- Yin, W., Wu, X. & Rui, X. Adaptive robust backstepping control of the speed regulating differential mechanism for wind turbines. *IEEE Trans. Sustain. Energy* **10**(3), 1311–1318. <https://doi.org/10.1109/TSTE.2018.2865631> (2019).
- Beniysa, M., El Janati El Idrissi, A., Bouajaj, A., Réda Britel, M. & Ariwa, E. Neural network adaptive backstepping control via uncertainty compensation for PMSG-based variable-speed wind turbine: Controller design and stability analysis. *Wind Eng.* <https://doi.org/10.1177/0309524X211031269> (2021).
- Matraji, I., Al-Durra, A. & Errouissi, R. Design and experimental validation of enhanced adaptive second-order SMC for PMSG-based wind energy conversion system. *Int. J. Electr. Power Energy Syst.* **103**, 21–30. <https://doi.org/10.1016/j.ijepes.2018.05.022> (2018).
- Xiong, L., Li, P., Ma, M., Wang, Z. & Wang, J. Output power quality enhancement of PMSG with fractional order sliding mode control. *Int. J. Electr. Power Energy Syst.* **115**, 105402. <https://doi.org/10.1016/j.ijepes.2019.105402> (2020).
- Hostettler, J. & Wang, X. Sliding mode control of a permanent magnet synchronous generator for variable speed wind energy conversion systems. *Syst. Sci. Control Eng.* **3**(1), 453–459. <https://doi.org/10.1080/21642583.2015.1082513> (2015).
- K. K. Gautam and V. Sankaranarayanan, Sliding mode control of surface mounted permanent magnet synchronous generator, vol. 3, no. PART 1. IFAC, 2014.
- M. Ayadi, F. Ben Salem, and N. Derbel, “Sliding mode approach for blade pitch angle control wind turbine using PMSG under DTC,” 16th Int. Conf. Sci. Tech. Autom. Control Comput. Eng. STA 2015, no. December 2018, pp. 758–762, 2016, doi: <https://doi.org/10.1109/STA.2015.7505131>.
- Benelghali, S., Benbouzid, M. E. H., Charpentier, J. F., Ahmed-Ali, T. & Munteanu, I. Experimental validation of a marine current turbine simulator: Application sliding mode control. *IEEE Trans. Ind. Electron.* **58**(1), 118–126. <https://doi.org/10.1109/TIE.2010.2050293> (2011).
- Errouissi, R. & Al-Durra, A. A novel PI-type sliding surface for PMSG-based wind turbine with improved transient performance. *IEEE Trans. Energy Convers.* **33**(2), 834–844. <https://doi.org/10.1109/TEC.2017.2776752> (2018).
- Phan, D. H. & Huang, S. D. Super-twisting sliding mode control design for cascaded control system of pmsg wind turbine. *J. Power Electron.* **15**(5), 1358–1366. <https://doi.org/10.6113/JPE.2015.15.5.1358> (2015).
- Yin, X. *et al.* A novel fuzzy integral sliding mode current control strategy for maximizing wind power extraction and eliminating voltage harmonics. *Energy, Elsevier* **85**(4), 677–686 (2015).
- Manale B, Badre B, Hala AA, et al (2020) DEADBEAT control applied towind power system. 2020 5th Int Conf Renew Energies Dev Countries, REDEC 2020 5: <https://doi.org/10.1109/REDEC49234.2020.9163601>

25. Jaramillo-Lopez, F., Kenne, G. & Lamnabhi-Lagarrigue, F. A novel online training neural network-based algorithm for wind speed estimation and adaptive control of PMSG wind turbine system for maximum power extraction. *Renew Energy* **86**, 38–48 (2016).
26. El Mourabit, Y. *et al.* Sustainable production of wind energy in the main Morocco's sites using permanent magnet synchronous generators. *Int. Trans. Electr. Energy Syst.* **30**, e12390 (2020).
27. Meghni, B., Dib, D. & Azar, A. T. A second-order sliding mode and fuzzy logic control to optimal energy management in wind turbine with battery storage. *Neural Comput. Appl.* **28**, 1417–1434 (2017).
28. Benamor, A., Benchouia, M. T., Srairi, K. & Benbouzid, M. E. H. A new rooted tree optimization algorithm for indirect power control a wind turbine based on a powered double induction generator. *ISA Trans.* **88**, 296–306 (2019).
29. Beltran, B., Benbouzid, M. E. H. & Ahmed-Ali, T. Second-order sliding mode control of a doubly fed induction generator driven wind turbine. *IEEE Trans. Energy Convers.* **27**(2), 261–269 (2012).
30. Yang, Bo., Tao, Yu., Shu, H., Dong, J. & Jiang, L. Robust sliding-mode control of wind energy conversion systems for optimal power extraction via non-linear perturbation observers. *Appl. Energy (Elsevier)* **210**, 711–723 (2018).
31. Freire, N., Estima, J. & Cardoso, A. A comparative analysis of PMSG drives based on vector control and direct control techniques for wind turbine applications. PRZEGLĄD ELEKTROTECHNICZNY (Electrical Review), ISSN 0033–2097, R. 88 NR 1a/2012.
32. Zribi, M., Alrifai, M. & Rayan, M. Sliding mode control of a variable- speed wind energy conversion system using a squirrel cage induction generator. *Energies* **10**, 604 (2017).
33. Gonzalez, L., Figueres, E., Garcera, G. & Carranza, O. Maximum-power-point tracking with reduced mechanical stress applied to wind energy conversion systems. *Appl. Energy* **87**, 2304–2312 (2010).
34. Mousa, H. H., Youssef, A. R. & Mohamed, E. E. Model predictive speed control of five-phase permanent magnet synchronous generator-based wind generation system via wind-speed estimation. *Int. Trans. Electr. Energy Syst.* **29**(5), e2826 (2019).
35. Jena, N. K., Mohanty, K. B., Pradhan, H. & Sanyal, S. K. A comparison between PI SMC used for decoupled control of PMSG in a variable speed wind energy system. In *2015 International Conference on Energy, Power and Environment: Towards Sustainable Growth (ICEPE)*; 2015. p. 1–6.
36. Jin, N., Wang, X. & Wu, X. Current sliding mode control with a load sliding mode observer for permanent magnet synchronous machines. *J. Power Electron.* **14**(1), 105–114 (2014).
37. Bossoufi, B. *et al.* Observer Backstepping control of DFIG-generators for wind turbines variable-speed: FPGA-based implementation. *Renew. Energy J.* **81**, 903–917 (2015).
38. Rhaili, S. E., Abbou, A., Marhraoui, S., Moutchou, R. & El Hichami, N. Robust sliding mode control with five sliding surfaces of five-phase PMSG based variable speed wind energy conversion system. *Int. J. Intell. Eng. Syst.* **13**(4), 346–357 (2020).
39. Bouderbala, M. *et al.* Experimental validation of predictive current control for DFIG: FPGA implementation. *Electronics* **10**(21), 2670. <https://doi.org/10.3390/electronics10212670> (2021).
40. Bossoufi, B. *et al.* Rooted tree optimization for Backstepping power control of DFIG wind turbine: dSPACE implementation. *IEEE Access* **9**(1), 26512–26522 (2021).
41. AlamiAroussi, H., Ziani, E. M., Bouderbala, M. & Bossoufi, B. Enhancement of the direct power control applied to DFIG-WECS. *Int. J. Electr. Comput. Eng.* **10**(1), 1511–1520 (2020).
42. Hammoumi, D. *et al.* Direct controls for wind turbine with PMSG used on the real wind profile of Essaouira-Morocco city. *Indones. J. Electr. Eng. Comput. Sci.* **16**(3), 1229–1239 (2019).
43. Alami Aroussi, H., Ziani, E. M., Bouderbala, M. & Bossoufi, B. Improvement of direct torque control applied to doubly fed induction motor under variable speed. *IJPEDS Int. J. Power Electron. Drive Syst.* **11**(1), 1511–1520 (2020).
44. El Mahfoud, M., Bossoufi, B., El Ouanjli, N., Mahfoud, S. & Taoussi, M. Improved direct torque control of doubly fed induction motor using space vector modulation. *Int. J. Intell. Eng. Syst.* **14**(3), 177–188 (2021).
45. ElKaraoui, I., Maaroufi, M. & Bossoufi, B. Fuzzy sliding mode power control for wind power generation system connected to the grid. *IJPEDS Int. J. Power Electron. Drive Syst.* **11**(4), (2021).
46. El Mahfoud, M., Bossoufi, B., El Ouanjli, N., Mahfoud, S. & Taoussi, M. Three speed controllers of direct torque control for a doubly fed induction motor drive: A comparison. *ELECTRICA* **21**, 129–141 (2021).
47. Majout, B. *et al.* Improvement of sliding mode power control applied to wind power generation system based on DFIG. *IJPEDS Int. J. Power Electron. Drive Syst.* **12**(1), 441–452 (2021).
48. Zine Laabidine, N., Errarhout, A., El Bakkali, C., Karim, M. & Bossoufi, B. Sliding mode control design of wind power generation system based on PMSG. *IJPEDS Int. J. Power Electron. Drive Syst.* **12**(1), 393–403 (2021).
49. Alami, H. E. *et al.* FPGA in the loop implementation for observer sliding mode control of DFIG-generators for wind turbines. *Electronics* **11**, 116. <https://doi.org/10.3390/electronics11010116> (2022).

## Author contributions

Conceptualization, F.E.; methodology, F.E.; software, Y.I.; validation, Y.I, B.B; formal analysis, FE; investigation, F.E, M.M, S.A; resources, M.B; data curation, F.E writing—original draft preparation, M.B; writing—review and editing, S.M, M.G, M.M, S.A; visualization, B.B; supervision, B.B, M.B, S.M; project administration, B.B, M.M, S.A; Funding, S.M, M.M, S.A. All authors reviewed the manuscript.

## Funding

This work was supported by Taif University Researchers Supporting Project (TURSP) under number (TURSP-2020/73), Taif University, Taif, Saudi Arabia.

## Competing interests

The authors declare no competing interests.

## Additional information

**Correspondence** and requests for materials should be addressed to B.B.

**Reprints and permissions information** is available at [www.nature.com/reprints](http://www.nature.com/reprints).

**Publisher's note** Springer Nature remains neutral with regard to jurisdictional claims in published maps and institutional affiliations.



**Open Access** This article is licensed under a Creative Commons Attribution 4.0 International License, which permits use, sharing, adaptation, distribution and reproduction in any medium or format, as long as you give appropriate credit to the original author(s) and the source, provide a link to the Creative Commons licence, and indicate if changes were made. The images or other third party material in this article are included in the article's Creative Commons licence, unless indicated otherwise in a credit line to the material. If material is not included in the article's Creative Commons licence and your intended use is not permitted by statutory regulation or exceeds the permitted use, you will need to obtain permission directly from the copyright holder. To view a copy of this licence, visit <http://creativecommons.org/licenses/by/4.0/>.

© The Author(s) 2022